ELSEVIER

Journal of Power Sources 110 (2002) 86–90

JOURNAL OF POWER SOURCES

www.elsevier.com/locate/jpowsour

Characterization of $RuO_2 \cdot xH_2O$ with various water contents

J.P. Zheng[a,*], Y. Xin[b]

[a]*Department of Electrical and Computer Engineering, Florida A&M University and Florida State University, Tallahassee, FL 32310, USA*

[b]*Magnet Science and Technology, National High Magnetic Field Laboratory, Florida State University, Tallahassee, FL 32310, USA*

Received 14 March 2002; accepted 30 March 2002

Abstract

Hydrous ruthenium oxides ($RuO_2 \cdot xH_2O$) with different contents of water (x) were prepared by annealing commercial $RuO_2 \cdot 2.6H_2O$ powders at different temperatures. The morphologies and crystalline structures of $RuO_2 \cdot xH_2O$ were investigated using transmission electron microscope (TEM) and selected area electron diffraction (SAED) techniques. From the TEM images, it was observed that the particle size of $RuO_2 \cdot xH_2O$ increased with increasing annealing temperature. From the SAED patterns, it was observed that $RuO_2 \cdot xH_2O$ powders became an amorphous phase at annealing temperatures <116 °C and became a crystalline phase at annealing temperatures above 116 °C. Amorphous $RuO_2 \cdot xH_2O$ prepared at 116 °C reached its maximum specific capacitance as a result of proton insertion into the bulk of RuO_2 but with smaller Ru–Ru distance in the local structure. The more disordered structure induced by proton insertion was obtained by SAED pattern from a sample annealed at 116 °C. The possible connection between the microstructure and specific capacitance of $RuO_2 \cdot xH_2O$ is discussed.

Keywords: Hydrous ruthenium oxide; Transmission electron microscope; Selected area electron diffraction

1. Introduction

Hydrous ruthenium oxides ($RuO_2 \cdot xH_2O$) were found to be able to store more proton than anhydrous ruthenium oxides [1,2]. The proton density in $RuO_2 \cdot xH_2O$ was strongly dependent on the structure of the hydrous ruthenium oxide and the annealing temperature during the sample preparation. The specific capacitance [3] of 900 F/g and interfacial capacitance [4] of over 4 F/cm^2 were obtained from powder and thin film of amorphous ruthenium oxides, respectively. The specific capacitance was found to be insensitive to the specific surface area but sensitive to the crystalline structure [2]. It was found that $RuO_2 \cdot xH_2O$ with the maximum specific capacitance was always obtained at the temperature near the phase transition from amorphous to crystalline [2,5,6]. From previous studies, it is believed that the superior specific capacitance in amorphous $RuO_2 \cdot xH_2O$ has an unexpectedly high degree of proton insertion into the bulk materials. By contrast, for crystalline RuO_2, bulk materials typically are limited to surface interaction with proton [7,8], resulting in a lower specific capacitance. However, there is still a lack of direct evidence to support this theory. Several non-electrochemical techniques were also involved in studying the charge storage mechanisms in $RuO_2 \cdot xH_2O$, including X-ray fine structure analysis (EXAFS) [3] and nuclear magnetic resonance [11]. In this paper, we report recent studies on $RuO_2 \cdot xH_2O$ microstructures and structural changes after proton insertion in samples prepared at different annealing temperatures by means of transmission electron microscopy (TEM).

2. Experimental

Experimental samples of $RuO_2 \cdot xH_2O$ were prepared by annealing commercial $RuO_2 \cdot 2.76H_2O$ powders (Alfa) in an air circulation oven for about 24 h. Samples with different water contents (x) and crystalline structures were obtained after annealing at different temperatures. Values of x were calculated from the weight change of annealed samples.

The specific capacitance reported in this paper was measured by cyclic voltrammogram (CV). To prepare a $RuO_2 \cdot xH_2O$ electrode, Teflon emulsion (60% solid) as a binder was first mixed with the $RuO_2 \cdot xH_2O$ powder. The mixture was then rolled into a film 100–200 μm thick, from which a square of about 0.4 cm × 0.4 cm was cut. The platinum grid was then pressed into the square from both

* Corresponding author. Tel.: +1-850-410-6464; fax: +1-850-410-6479.
E-mail address: zheng@eng.fsu.edu (J.P. Zheng).

0378-7753/02/$ – see front matter
PII: S0378-7753(02)00234-3

sides for mechanical support and current collection. Three-electrode cells were used for CV experiments. The working electrode was formed from Teflon bound $RuO_2{\cdot}xH_2O$ powders. The counter electrode was made of a Pt grid of a size much larger than that of the working electrode. A standard saturated calomel electrode (SCE) (+0.2412 V versus the standard hydrogen electrode) was used as the reference electrode. Aqueous solutions of 0.5 M H_2SO_4 were used for the electrolyte. The electrolyte was bubbled with nitrogen gas for at least 30 min before any electrochemical measurement was made.

In order to characterize the $RuO_2{\cdot}xH_2O$ materials before and after proton insertion on a microscopic scale, two groups of TEM samples were studied. The first group of samples was prepared by pressing the thin carbon film coated TEM Cu mesh grid into the dry $RuO_2{\cdot}xH_2O$ powders, by which the sample powder particles are attached to the carbon film. The second group of samples was prepared by mixing powders in methanol to form a suspension, and then the TEM sample was made by dipping the TEM carbon grid into the suspension, and letting it dry in air. Samples were investigated by a JEOL-2010 TEM system, operated at 200 kV, with a resolution of 0.23 nm. In order to prevent electron irradiation damage (i.e. sample heating) and contamination, a weak illumination condition and cold trap were used. The selected area electron diffraction (SAED) pattern was employed to analyze the crystallinity.

3. Results and discussion

Table 1 listed annealing conditions and some properties of experimental samples used in this study. The water content (x) in the structure of $RuO_2{\cdot}xH_2O$ decreased with increasing annealing temperature due to the simple thermal dehydration; however, the specific capacitance increased initially, and reached a peak value at 116 °C, then decreased when the annealing temperature further increased. The capacitance was measured by the CV method at a voltage scan rate of 2 mV/s. The maximum specific capacitance of 617 F/g was obtained at 116 °C. The dependence of the specific capacitance on annealing temperature is similar to previous observations that were obtained from the $RuO_2{\cdot}xH_2O$ samples prepared by a sol–gel method [4]. However, the maximum value of the specific capacitance is less than previously [2,3]. It was found that the maximum value of the specific capacitance was sensitive to the preparation conditions such as impurity concentration [2,6], pH value during the sol–gel process [2] and structural water content. Even for commercial $RuO_2{\cdot}xH_2O$ powders, different maximum values of specific capacitance would be obtained from separately purchased batches. But regardless of the absolute value of specific capacitance, the peak value was always obtained from the samples that were annealed near the temperature at which the phase transition from amorphous to crystalline occurred.

The open circuit potential (VOC) of each sample was measured and listed in Table 1. VOC_1 and VOC_2 were measured for samples that were prepared from dry powder and methanol suspensions, respectively. A large potential shift in the negative direction was obtained for samples prepared from a methanol suspension. The potential shift was believed to be due to the chemical reaction between $RuO_2{\cdot}xH_2O$ powders and methanol solvent when they were mixed. It is believed that the chemical reaction is similar to the methanol oxidation reaction that occurs on the anode catalyst of direct methanol fuel cells [12,13]. During the oxidation process, protons were inserted into the bulk of amorphous $RuO_2{\cdot}xH_2O$ or adsorbed at the surface of crystalline $RuO_2{\cdot}xH_2O$. This process is called protonation. Based on the assumption that the Ru valence state changes from $Ru^{2+}(OH)_2$ at about 0 V to $Ru^{4+}O_2$ at about 1.4 V versus the standard hydrogen electrode [9,10] and the proton-ruthenium reaction rate occurs uniformly in the potential range, then the average proton content in the electrode after protonation reaction can be estimated according to the VOC_2 values. Samples of $RuO_{0.907}(OH)_{1.093}{\cdot}2.65H_2O$, $RuO_{0.941}(OH)_{1.059}{\cdot}0.76H_2O$, and $RuO_{1.054}(OH)_{0.946}{\cdot}0.06H_2O$ were prepared without thermal treatment, and were annealed at 150 and 300 °C. It can be seen from Table 1 that average values of Ru valence state for protonated samples were about Ru^{3+}. It must be pointed out that the sample preparation process must be very carefully controlled. It was found that the chemical reaction could cause ignition if the reaction rate was not controlled. The reaction was an exothermic one. If the heat energy is released quickly, then the temperature of the methanol would be raised to the flammable point. Therefore, in this experiment, $RuO_2{\cdot}xH_2O$ powders were very slowly added methanol in order to control the temperature rise due to the reaction.

Table 1
Summary of some properties of $RuO_2{\cdot}xH_2O$ samples as a function of annealing temperature

Annealing temperature	Without thermal treatment	116 °C	300 °C
As annealed	$RuO_2{\cdot}2.76H_2O$	$RuO_2{\cdot}0.60H_2O$	$RuO_2{\cdot}0.06H_2O$
VOC_1	0.873 V vs. SCE	0.977 V vs. SCE	0.884 V vs. SCE
Structure	Amorphous	Amorphous	Crystalline
Specific capacitance	207 F/g	617 F/g	182 F/g
VOC_2	0.481 V vs. SCE	0.459 V vs. SCE	0.564 V vs. SCE
After protonation	$RuO_{0.97}(OH)_{1.03}{\cdot}2.65H_2O$	$RuO_{1.0}(OH)_{1.0}{\cdot}0.76H_2O$	$RuO_{1.15}(OH)_{0.85}{\cdot}0.06H_2O$

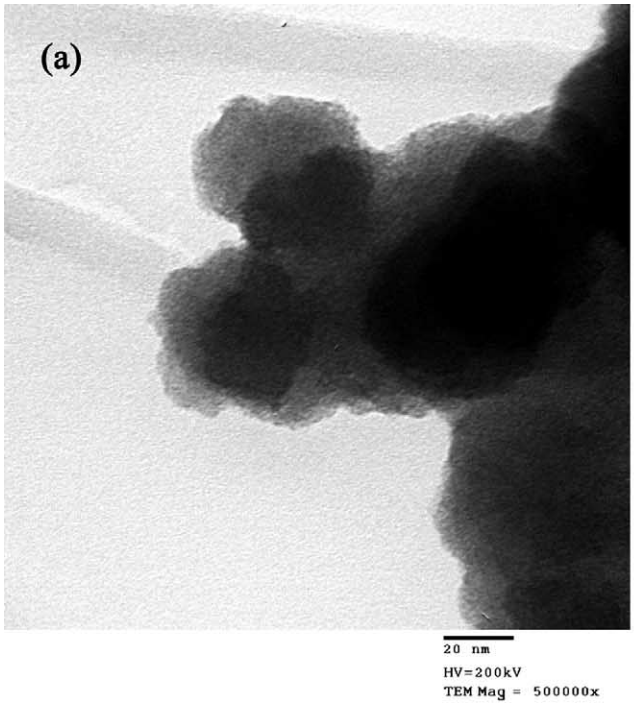

Fig. 1. (a) TEM image, and (b) SAED pattern from the sample of $RuO_2{\cdot}2.76H_2O$.

The first TEM measurement was conducted on samples without protonation. Fig. 1(a and b) show the TEM image and SAED pattern from $RuO_2{\cdot}2.76H_2O$, respectively. It can be seen from Fig. 1(a) that the $RuO_2{\cdot}2.76H_2O$ was formed in particles mostly with a size of about 50 nm, which is about two times larger than reported previously [2], in which a diameter of a spherical particle is used to estimate the size of the particle based on the measurement of the specific surface area. The difference can be explained by the fact that the surface of the particles is quite rough as can be seen from the TEM image, which resulted in an actual specific surface area

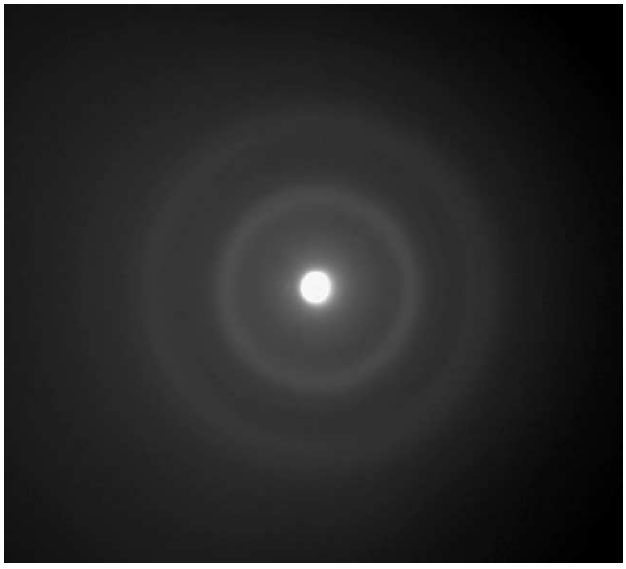

Fig. 2. The SAED pattern measured from the sample of $RuO_2{\cdot}0.60H_2O$ prepared at 116 °C.

larger than that based on a smooth sphere particle model. From Fig. 1(b), the characteristic feature of the diffraction pattern that has one broad-ring and a diffuse background indicated that $RuO_2{\cdot}2.76H_2O$ is an amorphous phase material. The position of the maximum of the ring corresponded to real space distance of 0.25 nm. However, further quantitative analysis of the diffraction data through Fourier transform is needed to obtain the nearest neighbor correlation distances and coordination numbers.

Fig. 2 shows the SAED pattern from $RuO_2{\cdot}0.60H_2O$ annealed at 116 °C. The real space distance was 0.22 nm from the position of the maximum of the ring. From Fig. 2, it can be concluded that the $RuO_2{\cdot}0.60H_2O$ was still an amorphous phase. The larger diameter of the first ring compared to the sample without thermal annealing indicate the shorter distance of the nearest neighbors of Ru–Ru atoms in the clusters. It became progressively more ordered in local structure than without thermal annealing. Fig. 3(a and b) were obtained from $RuO_2{\cdot}0.06H_2O$ prepared at 300 °C. From Fig. 3(a), it can also be seen that in each cluster a large number of crystalline RuO_2 with size <5 nm were formed. The orientations of the nano-sized crystals were random; however, the size of the crystals increased with increasing annealing temperature. In Fig. 3(b), there are three rings present, and they corresponded to (1 1 0), (1 0 1) and (1 2 1) of the rutile RuO_2 structure. At 500 °C, larger crystalline RuO_2 particles were formed (Fig. 4).

Similar measurements were also performed on protonated samples after the chemical reaction with methanol. For samples prepared at 25 and 300 °C, no difference was observed for both TEM image and SAED pattern from the samples with and without a protonation process. However, a different SAED pattern was obtained for the protonated sample annealed at 116 °C as shown in Fig. 5. By comparing SAED patterns in Figs. 2 and 5, it can be seen that the

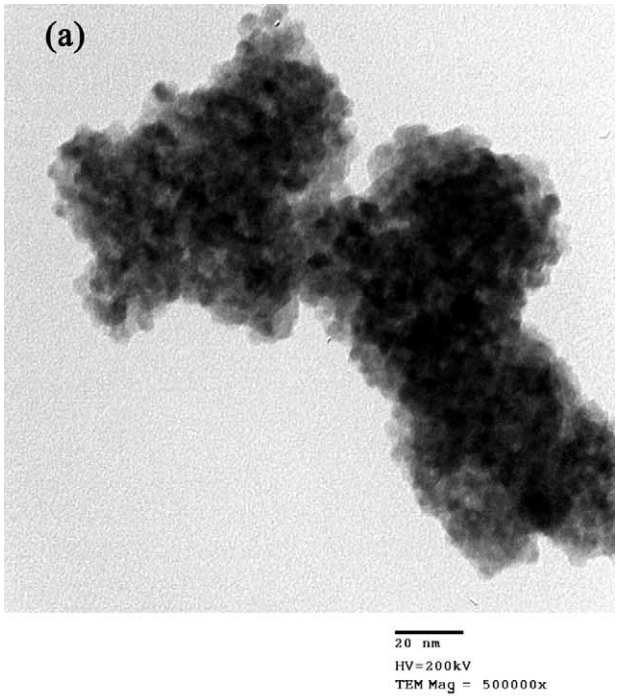

Fig. 3. (a) TEM image, and (b) SAED pattern from the crystalline $RuO_2{\cdot}0.06H_2O$ prepared at 300 °C.

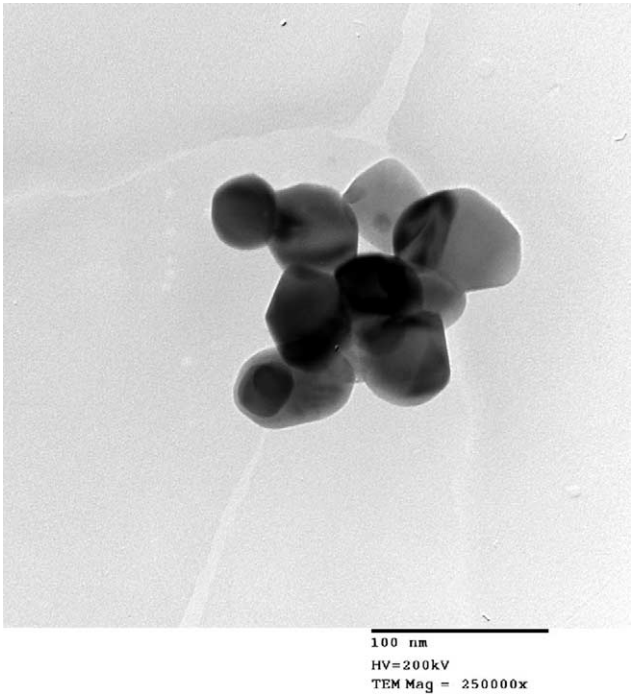

Fig. 4. TEM image of RuO_2 sample annealed at 500 °C.

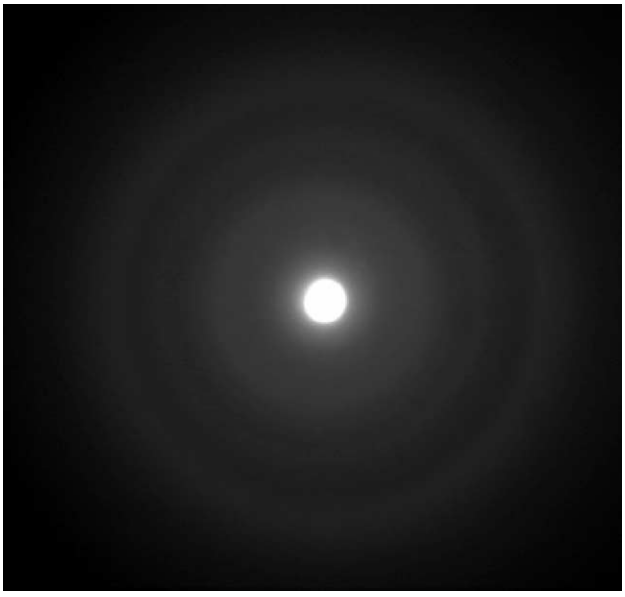

Fig. 5. SAED pattern measured from $RuO_{1.0}(OH)_{1.0}{\cdot}0.60H_2O$ that was annealed at 116 °C and then reacted with methanol.

diffraction ring from a protonated sample was more diffuse and broader than that from non-protonated samples. The changes of SAED patterns from samples with and without pontonation processes can be explained as follows:

1. For the sample of $RuO_2{\cdot}2.76H_2O$, the structure of ruthenium oxide was filled with larger member of H_2O molecules. The broadring in the SAED pattern indicated that the sample was highly disordered. The EXAFS study [3] also proved that no three-dimensional (3D) networks of linked RuO_6 octahedral chains existed in $RuO_2{\cdot}xH_2O$ with a high structural water content. The same SAED pattern observed on the $RuO_2{\cdot}2.76H_2O$ sample before and after protonation can be understood if the proton insertion into $RuO_2{\cdot}2.76H_2O$ did not cause further disorder in an already highly disordered lattice, and further disorder in the lattice could not be detected within the resolution of SAED pattern.
2. For the sample of $RuO_2{\cdot}0.60H_2O$, a local structure of RuO_2 was formed. The EXAFS study also showed that

no long-range order of RuO_2 structure was formed; however, the local structure consist of rutile RuO_6 octahedred interconnected in chains. From the OCV_2 potential measurements of protonated samples, it was found about 50% of Ru–O bonds were converted to Ru–OH bonds after protons were inserted into the $RuO_2{\cdot}xH_2O$ structure. The proton insertion process caused an inhomogeneous lattice expansion and greater degree of disordering, which was reflected by the broadening of the diffraction ring in the SAED pattern. Therefore, the broadening in the SAED pattern is direct evidence of proton insertion into the bulk of amorphous $RuO_2{\cdot}xH_2O$.

3. For the sample of crystalline $RuO_2{\cdot}0.06H_2O$, a 3D network of RuO_6 octahedral chains was formed. The proton was not able to insert into the bulk of crystal but only react with the Ru ion at the surface of the crystal. Therefore, the protonation process did not affect the crystalline structure of RuO_2.

The microstructural changes with increasing annealing temperature directly affect the specific capacitance of $RuO_2{\cdot}xH_2O$ samples. It is believed that the proton diffusion can only occur in the amorphous phase of $RuO_2{\cdot}xH_2O$ and is dependent on the Ru–Ru distance. For $RuO_2{\cdot}xH_2O$ samples prepared at low annealing temperatures, the Ru–Ru distance was relatively large due to the high structural water content (e.g. $x = 2.76$ at $T_{anneal} = 25\ ^\circ C$), which isolated the Ru ions from each other. SAED and EXAFS [3] results proved that $RuO_2{\cdot}xH_2O$ prepared at 25 °C had no short-range order. Therefore, to transport a proton from one Ru site to another was rather difficult. For the $RuO_2{\cdot}xH_2O$ sample annealed at 116 °C, the Ru–Ru distance decreased while the water content was reduced to $x = 0.6$. The SAED results indicated that the Ru–Ru distance is indeed shorter in the local structure. The proton could be diffused easily into $RuO_2{\cdot}0.60H_2O$. Finally for the samples annealed at temperatures above 116 °C, the crystalline structure was formed. The lattice of crystalline RuO_2 was too rigid to allow proton insertion, which prohibited proton diffusion. Only the Ru ions at the crystal surface involved the protonation process. Therefore, the $RuO_2{\cdot}0.60H_2O$ sample annealed at 116 °C, which contained the lowest structural water in the amorphous phase of $RuO_2{\cdot}xH_2O$, has the highest specific capacitance. The recent study [14] on ^1H nuclear magnetic resonance spectroscopy at various temperatures also showed a strong correlation between the activation energy of protons and the specific capacitance of $RuO_2{\cdot}xH_2O$. A minimum value of activation energy was obtained from the sample annealed at 116 °C, which indicated that the potential barrier was low and protons could be easily diffused into and out of the bulk of the $RuO_2{\cdot}xH_2O$ sample.

4. Conclusion

The $RuO_2{\cdot}xH_2O$ samples with various water contents were studied by TEM SAED, and electrochemical measurements. For samples without thermal treatment, $RuO_2{\cdot}xH_2O$ was amorphous. The structure contained larger amounts of water and larger Ru–Ru distances. After annealed at a temperature of 116 °C, the sample possesses the highest specific capacitance. Smaller Ru–Ru distances in the local structure formed; however, the structure became more disordered by proton intercalation. At high temperatures, crystalline RuO_2 was obtained, and the proton intercalation was prevented.

Acknowledgements

The authors thank X. Wang for performing the open circuit potential measurements. This research was supported partially by the NASA under Grant No. NAG5-9420.

References

[1] J.P. Zheng, T.R. Jow, J. Electrochem. Soc. 142 (1995) L6.
[2] J.P. Zheng, P.J. Cygan, T.R. Jow, J. Electrochem. Soc. 142 (1995) 2695.
[3] D.A. McKeown, P.L. Hagans, L.P.L. Carette, A.E. Russell, K.E. Swider, D.R. Rolison, J. Phys. Chem. B 103 (1999) 4825.
[4] Q.L. Fang, D.A. Evans, S.L. Roberson, J.P. Zheng, J. Electrochem. Soc. 148 (2001) A833.
[5] I.H. Kim, K.B. Kim, Electrochem. Solid-State Lett. 5 (2001) A62.
[6] Y.U. Jeong, A. Manthiram, Electrochem. Solid-State Lett. 3 (2000) 205.
[7] I.D. Raistrick, R.J. Sherman, in: S. Srinivasan, S. Wagner, H. Wroblowa (Eds.), Proceedings of the Electrochemical Society Series on Materials and Processes for Energy Conversion and Storage, PV 87–12, Pennington, NY, 1987, p. 582.
[8] H.B. Sierra Alcazar, K.A. Kern, G.E. Mason, R. Tong, Proceedings of the Thirty-third Power Sources Symposium at The Electrochemical Society Inc., Cherry Hill, NJ, 13–16 June 1988, p. 607.
[9] S. Trasatti, G. Lodi, in: S. Trasatti (Ed.), Electrodes of Conductive Metallic Oxides: Part A, Elsevier, New York, 1980, p. 301.
[10] S. Hadzi-Jordanov, H. Angerstein-Kozlowska, M. Vukovic, B.E. Conway, J. Electrochem. Soc. 125 (1978) 1471.
[11] Z.R. Ma, J.P. Zheng, R.Q. Fu, Chem. Phys. Lett. 331 (2000) 64.
[12] J.B. Goodenough, A. Hamnett, B.J. Kennedy, R. Manoharan, S.A. Weeks, J. Electroanal. Chem. 240 (1988) 133.
[13] D. Chu, S. Gilman, J. Electrochem. Soc. 143 (1996) 1685.
[14] R.Q. Fu, Z.R. Ma, J.P. Zheng, J. Phys. Chem. B 106 (2002) 3592.